

FRB event rate predictions for the Ooty Wide Field Array

Siddhartha Bhattacharyya¹*, Apurba Bera^{3†},
Somnath Bharadwaj^{1,2}, N. D. Ramesh Bhat^{4,5}
and Jayaram N. Chengalur³

¹ *Department of Physics, Indian Institute of Technology, Kharagpur, 721302, India*

² *Centre for Theoretical Studies, Indian Institute of Technology, Kharagpur, 721302, India*

³ *National Centre for Radio Astrophysics, Tata Institute of Fundamental Research, Pune 411007, India*

⁴ *International Centre for Radio Astronomy Research, Curtin University, Bentley, WA 6102, Australia*

⁵ *Australian Research Council Centre of Excellence for All-Sky Astrophysics (CAASTRO)*

Abstract. We developed a generic formalism to estimate the event rate and the redshift distribution of Fast Radio Bursts (FRBs) in our previous publication (Bera et al. 2016), considering FRBs are of an extragalactic origin. In this paper we present (a) the predicted pulse widths of FRBs by considering two different scattering models, (b) the minimum total energy required to detect events, (c) the redshift distribution and (d) the detection rates of FRBs for the Ooty Wide Field Array (OWFA). The energy spectrum of FRBs is modelled as a power law with an exponent $-\alpha$ and our analysis spans a range $-3 \leq \alpha \leq 5$. We find that OWFA will be capable of detecting FRBs with $\alpha \geq 0$. The redshift distribution and the event rates of FRBs are estimated by assuming two different energy distribution functions; a Delta function and a Schechter luminosity function with an exponent $-2 \leq \gamma \leq 2$. We consider an empirical scattering model based on pulsar observations (model I) as well as a theoretical model (model II) expected for the intergalactic medium. The redshift distributions peak at a particular redshift z_p for a fixed value of α , which lie in the range $0.3 \leq z_p \leq 1$ for the scattering model I and remain flat and extend up to high redshifts ($z \lesssim 5$) for the scattering model II.

Key words: cosmology: observations.

*Email:siddhartha@phy.iitkgp.ernet.in

†Email:apurba@ncra.tifr.res.in

1. Introduction

Fast Radio Bursts (FRBs) are highly-dispersed, millisecond duration pulses, discovered at the Parkes radio telescope (Thornton et al. 2013 & Lorimer et al. 2007). The high dispersion measures (DM) of the detected FRBs often show $\sim 5 - 20$ times excess DMs compared to what is expected from the model for the electron density distribution in our Galaxy (Cordes & Lazio 2002), thereby strongly suggesting they are extragalactic phenomena. The observed dispersion and scattering indices are believed to be due to propagation through cold ionized plasma of the interstellar medium (ISM) of our Galaxy, the host galaxy of the FRB and the intergalactic medium (IGM). If they indeed originate from cosmological distances, FRBs arise in extremely energetic sources with energies $\sim 10^{33} - 10^{35}$ J being released over timescales of a few milliseconds.

A total of 26 FRBs have been discovered over the past decade, of which 17 are reported in the published literature (Petroff et al. 2016). Of these 15 have been detected at the Parkes radio telescope and one each at the Arecibo radio telescope and the Green Bank radio telescope (GBT). One of the FRBs has been found to repeat (Spitler et al. 2016), where 10 detections from the same source have been recorded by two different observations separated by about two weeks. This suggests that there could be more than one type of progenitors for FRBs.

There are several proposed models for the emission mechanism of FRBs (Kulkarni et al. 2015), but as of yet there is no consensus as to which is the most likely scenario. The energy spectrum and the energy distribution of the events are also not well established. Estimates of the spectral index are available only for a few FRBs, but even then they are not reliably estimated given the poor localization possible with single-dish observations. A high positive spectral index in the range 7 to 11 is observed for FRB 121102 (Spitler et al. 2014) and a high negative spectral index (-7.8) is observed for FRB 110523 (Masui et al. 2015). Furthermore, a wide range of variation of spectral index (-10.4 to 13.6) has been observed for the repeated burst (Spitler et al. 2016). Moreover, two FRBs have been detected with circular polarization (Petroff et al. 2016).

In our previous work Bera et al (2016), we developed a generic formalism to estimate the event rates and the redshift distribution of FRBs detected by a given radio telescope. We considered two different scattering models to estimate the observed pulse width (w) and a power law $E_\nu \propto \nu^{-\alpha}$ for the energy spectrum of FRBs, where ν is the observing frequency. The energy distribution of FRBs is still unknown and we considered two possible energy distribution functions. For the purpose of this work, we consider FRBs to be one-off transient events (ignoring the repeating FRB, which is clearly an exception), which can be characterized by a single energy distribution. The model is normalized by considering FRB 110220 as the reference event,

which is the second brightest event (after FRB 010724, the so-called Lorimer burst) detected at the Parkes radio telescope and well characterized in terms of its dispersion measure, scattering and fluence properties. The estimated total energy ($E_0 = 5.4 \times 10^{33}$ J) of this FRB spectrum is considered as the reference energy. We however note that the value of E_0 estimated by using our model (Bera et al. 2016) with $\alpha = 1.4$, which is differed from the energy estimate given by Thornton et al. (2013) by a factor of 5.

As described in Bera et al. (2016) we consider the detection of four FRBs of Thornton et al. (2013) to estimate the event rates. In our formalism all redshifts are inferred from the observed DMs of the reported FRBs by considering a host galaxy contribution that is similar to the Milky Way. We found that the scattering time scale places an upper limit to redshift (z_c), up to which FRBs can be detected. We estimated the redshift distribution of FRBs for the Parkes radio telescope as well as FRB event rates for the three systems of the Ooty Wide Field Array with an incoherent beam formation.

This paper is a follow-up of our previous work (Bera et al. 2016) and we present a detailed analysis that is applicable for the upcoming Ooty Wide Field Array. The Ooty Wide Field Array (OWFA) will be a majorly upgraded version of the Ooty Radio Telescope, a $530\text{m} \times 30\text{m}$ parabolic cylinder with a linear feed array of dipole receptor elements at its focus, operating at a central frequency of 326.5 MHz. The signals from the individual elements can be combined and beam formed in two different ways, incoherent beam formation and a coherent single beam formation. In the case of coherent single beam formation (CA-SB), the voltage signals from the individual elements with phase are added directly and then squared to obtain total power. The field of view (FoV) is proportional to λ/D , where λ is the wavelength of the observation and D is the length of the largest baseline. Here the sensitivity is increased by a factor of N_A compared to the sensitivity achieved by a single element. N_A is total number of elements, where an element is a segment spanning 24 dipole antennas for OWFA Phase I and 4 dipole antennas for OWFA Phase II. In the case of incoherent beam formation (IA), the squares of the voltages from the individual elements are summed over to obtain the total power. This mode of beam formation does not contain any phase information. Here the FoV is proportional to λ/d , where d is the length of a single element. Note that, for parabolic dishes the field of view is proportional to λ/D_P , where D_P is the diameter of the parabolic dish, whereas for cylindrical reflectors, the field of view is $\pi \times \lambda/b \times \lambda/d$, where b and d are the dimensions along the parallel and perpendicular to the cylindrical axis respectively. In this case the sensitivity is increased by a factor of $\sqrt{N_A}$ compared to the sensitivity achieved by a single element. More information about the baselines of OWFA Phase I and Phase II can be found in Ali & Bharadwaj (2014).

We also consider here a third kind of beam formation, which we call coherent multiple beam formation, which is the mixture of IA and CA-

SB mentioned above. In coherent multiple beam formation (CA-MB), one forms the IA to obtain a large instantaneous field of view but at a relatively shallow sensitivity. When an event is detected in the IA mode, the high time resolution signals are recorded to eventually form multiple coherent beams offline in all possible directions. This will give us the sensitivity of the CA-SB, but with the field of view of the IA. This specific kind of strategy was first demonstrated in a pilot transient survey with the Giant Metrewave Radio Telescope (GMRT) by Bhat et al. (2013).

In this paper, we estimate the FRBs event rates followed by the predicted pulse widths, the minimum total energy required to detect events and the redshift distribution of FRBs for the OWFA. We then compare our results with another two cylindrical radio telescopes that are gearing up for FRB events, UTMOST and CHIME. UTMOST (Caleb et al. 2016) is a cylindrical radio telescope that operates at an observational frequency of 843 MHz whereas CHIME (Newburgh et al. 2014) is an upcoming radio interferometer, which will operate at an observational frequency 600 MHz.

We provide estimates for the detection rates for all three beam forming modes for OWFA along with UTMOST and CHIME. However, we are considering only the IA and CA-SB modes for detailed comparisons, as a realistic implementation of CA-MB modes (for OWFA) will be largely dictated by affordable computational resources. As mentioned earlier, in the case of OWFA, we also consider the possibility, where we get to take advantage of both wide FoV and the full sensitivity, i.e. the use of IA for wide FoV (at the expense of shallow searches), but then will go for high-quality signal detection via CA-MB for promising candidates. We however clarify that this is not equivalent to an all-time CA-MB search.

A brief outline of the paper is as follows. In Section 2, we present a short description of the Ooty Wide Field Array along with UTMOST and CHIME. The predictions for the FRB event rates for OWFA, UTMOST and CHIME are described in Section 3 and we discuss and summarize our results in Section 4.

2. The Ooty Wide Field Array

The Ooty Wide Field Array (OWFA) is an upgraded version of the Ooty Radio Telescope (ORT) that was built in early 70's (Swarup et al. 1971). ORT has a long cylindrical reflector of dimension $530\text{m} \times 30\text{m}$. It contains 1056 half wavelength linear dipoles along the focal line of the parabolic cylindrical reflector. Therefore, it is sensitive only to a single polarization component of the incident radiation. The signals from these dipoles are currently combined, using an analogue beam forming network and we refer to this as the Legacy System. The signals from all 1056 dipoles are essentially combined to effectively form a coherent beam.

The Legacy System operates at an observational frequency $\nu_0 = 326.5$ MHz ($\lambda = 0.91$ m) with bandwidth $B = 4$ MHz. The ongoing upgrade envisages two modes of operation; Phase I & Phase II. In Phase I, each set of 24 dipoles will be combined to form a single element, whereas in Phase II, each element will consist of 4 dipoles. Only 40 of the 44 such sets (half-modules) will be used in Phase I, whereas Phase II will make use of all 1056 dipoles in the form of 264 elements. The bandwidth of Phase I and Phase II are 19.2 MHz and 38.4 MHz respectively, centred at the same observational frequency of the ORT Legacy System. More technical information about OWFA can be found in Subrahmanyam et al. (2016). The parameters of OWFA that are relevant for this work are tabulated in Table 1.

In this work the primary beam patterns $B(\vec{\theta})$ of the current and the new phases of OWFA (Ali & Bharadwaj 2014) are assumed to be given by

$$B(\vec{\theta}) = \text{sinc}^2\left(\frac{\pi d\theta_x}{\lambda}\right) \text{sinc}^2\left(\frac{\pi b\theta_y}{\lambda}\right) \quad (1)$$

where, $b \times d$ is the aperture of a single element and (θ_x, θ_y) are components of $\vec{\theta}$ on the plane of the sky. Two other radio telescopes, UTMOST (Caleb et al. 2016) and CHIME (Newburgh et al. 2014), are quite similar to OWFA, comprising long cylindrical reflectors and operating at a single radio frequency (843 MHz and 600 MHz, respectively), though CHIME will be equipped to record data over a large bandwidth. The parameters of UTMOST and CHIME are also tabulated in Table 1.

The detection probability of FRBs largely depends on two factors, the field of view (FoV) and the sensitivity (A_S) of the telescope¹. A telescope with a large field of view and a high sensitivity will be capable of detecting FRBs in large numbers. Therefore, the product $\text{FoV} \times A_S$ is a useful indicator of the detection prospects of FRBs for any given radio telescope. This product is maximum for CHIME in the CA-MB mode, however the three telescopes operate at different frequencies and therefore highly complementary. All these three telescopes also have effectively higher FRB detection sensitivity than the Parkes radio telescope or the Arecibo radio telescopes. For example, for the Parkes radio telescope, $\text{FoV} \times A_S = 8.94 \times 10^{-4} \text{ deg}^2 \text{ Jy}^{-1}$, which is $\sim 10^3$ times smaller than that of OWFA in the CA-MB mode.

3. Predictions of FRB event rates

In this section, we briefly describe the method we use to predict the detection rates of FRBs followed by the estimation of the predicted pulse widths,

¹The sensitivity A_S is defined as the ratio of the gain G of a single element to the system temperature T_{sys} of the telescope

Telescope	Beam Formation	N_A	ν (MHz)	B (MHz)	$\Delta\nu_c$ (kHz)	A_S (Jy $^{-1}$)	FoV (deg 2)	FoV \times A_S (deg 2 Jy $^{-1}$)	
ORT Legacy System	–	1	326.5	4	125	0.023	0.18	0.004	
OWFA Phase I	IA	40		19.2	24	0.004	8.05	0.032	
	CA-SB					0.02	0.21	0.004	
	CA-MB					0.02	8.05	0.161	
OWFA Phase II	IA	264		38.4	48	0.001	47.93	0.048	
	CA-SB					0.022	0.18	0.004	
	CA-MB					0.022	47.93	1.054	
UTMOST	IA	352		843	31.25	781.25	0.003	7.8	0.023
	CA-SB						0.057	0.07	0.004
	CA-MB						0.057	7.8	0.445
CHIME	IA	1280	600	400	1000	0.003	132	0.4	
	CA-SB					0.099	0.29	0.029	
	CA-MB					0.099	132	13.1	

Table 1: We estimate the sensitivity of the telescope A_S by considering system temperatures of OWFA, UTMOST and CHIME as 150 K, 70 K and 50 K respectively. We consider here three kinds of beam formation, incoherent beam formation (IA), coherent single beam formation (CA-SB) and coherent multiple beam formation (CA-MB). The symbols N_A , ν , B , $\Delta\nu_c$ and FoV stand for number of elements, observational frequency, bandwidth, spectral channel width and field of view of the telescope. The efficiency of a single element $\eta = 0.6$ is assumed to be same for OWFA, UTMOST and CHIME.

minimum total energy required to detect events and the redshift distribution of FRBs for a given radio telescope.

Further details on the formalism employed are reported in our previous work Bera et al. (2016).

3.1 Pulse width

The observed pulse width w of a FRB at a redshift z with an intrinsic pulse width w_i is given by

$$w = \sqrt{w_{cos}^2 + w_{DM}^2 + w_{sc}^2} \quad (2)$$

where, w_{cos} , w_{DM} and w_{sc} are the contribution from the cosmic expansion, dispersion broadening and scatter broadening, respectively. The term w_{cos} arises here due to the cosmological expansion of the universe, which is the product of w_i and $(1 + z)$. The cold ionized medium of the ISM in our Galaxy as well as the host galaxy of the FRB and the IGM introduces

dispersion smearing and scatter broadening. The observed radio signal is assumed to be incoherently de-dispersed. This would leave a residual dispersive smearing corresponding to the channel width, viz. w_{DM} . The exact mechanism of the scattering in the intervening medium is still unknown and we consider here two different scattering models; the ones based on, Bhat et al. (2004) and Macquart & Koay (2013), and denote them as the scattering model I (Sc-I) and the scattering model II (Sc-II), respectively.

The scattering model I is an empirical fit to a large body of pulsar measurements in the Milky Way, which we have rescaled it for the intergalactic medium, and given by

$$\log w_{sc} = C_0 + 0.15 \log DM_{IGM} + 1.1 (\log DM_{IGM})^2 - 3.9 \log \nu \quad (3)$$

where C_0 is a normalization constant and we have used $C_0 = 3.2$ to rescale the scattering model for the intergalactic medium. DM_{IGM} and ν are the dispersion measure due to the intergalactic medium and the observational frequency of the radio telescope respectively.

The scattering model II is largely a theoretical framework by considering the turbulence in the intergalactic medium, and given by

$$w_{sc}(z) = \frac{k_{sc}}{\nu^4 Z_L} \int_0^z D_H(z') dz' \int_0^z (1+z')^3 D_H(z') dz' \quad (4)$$

where,

$$D_H(z) = (\Omega_m(1+z)^3 + \Omega_\Lambda)^{-1/2},$$

$$Z_L = (1+z)^2 \left[(1+z) - \sqrt{z(1+z)} \right]^{-1}$$

and we have used the normalization constant $k_{sc} = 8.5 \times 10^{13}$ ms MHz⁴. Both normalization constants C_0 and k_{sc} are estimated by considering the pulse width of the reference event FRB 110220, which is $w = 5.6$ ms at redshift $z = 0.8$ with an intrinsic pulse width $w_i = 1$ ms. Note that in Eqs. 3 and 4, we have used ν_0 in MHz, w_{sc} in ms and DM in pc cm⁻³.

Figure 1 shows w as a function of z for FRB detection using OWFA. The different components of w for the two scattering models and the predicted values of w for UTMOST and CHIME, are also shown in this figure.

Contribution from dispersion smearing can be significant at higher DMs; for example, for $DM = 1000$ pc cm⁻³, we find that the values of w_{DM} are 29.78 ms, 5.72 ms and 11.44 ms for Legacy System, OWFA Phase I and Phase II, respectively. These however contribute $\lesssim 1\%$ to the predicted pulse width of FRBs for OWFA. Therefore, w_{DM} makes negligible contribution to w but w_{sc} dominates at large z . As discussed above, w_{DM} depends on the channel width of the detection backend (spectrometer), whereas w_{sc} solely depends on the observational frequency. Therefore, Fig. 1 is similar for all

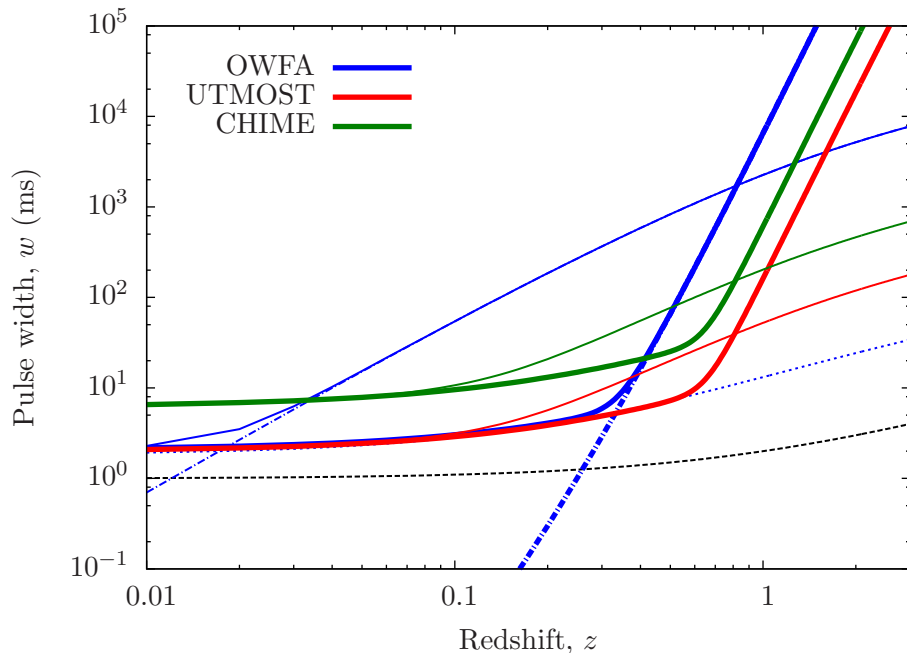


Figure 1: The predicted pulse width of a FRB located at a redshift z with intrinsic pulse width $w_i = 1$ ms (see text for details), assumed to be detected by using OWFA (Blue), UTMOST (Red) and CHIME (Green). The black dashed line refers the cosmic expansion, which is independent of the telescope configuration. The dotted and dot-dashed lines refer the dispersion broadening and the scatter broadening respectively. The thick and thin lines correspond to scattering model I (Sc-I) and scattering model II (Sc-II) respectively.

different modes of OWFA. The pulse width is independent of the rms noise and the field of view of the telescope. Thus, Fig. 1 is also similar for different modes of beam formation.

Figure 1 shows that the term w_{cos} makes an insignificant contribution to w for all redshifts for the assumed $w_i = 1$ ms. For the scattering model I, w_{sc} makes less contribution to w at low redshift ($z < 0.3$) in comparison with w_{DM} and it starts to dominate at $z \geq 0.3$. For the scattering model II, w_{sc} is very high and dominates w even at very low redshifts ($z \approx 0.03$). The value of w for the scattering model II is greater than that of the scattering model I up to $z \approx 0.8$, after which the latter one increases very sharply.

The predicted pulse widths for UTMOST and CHIME are smaller than those of OWFA, which follows from the fact that they operate at higher observing frequencies. However, the qualitative nature of the curves are similar to those of OWFA. We have repeated the entire analysis with different

values of w_i (0.5 ms & 2 ms). The normalization constants of both scattering models differ but the overall changes in w is negligible and hence do not affect the curves. It essentially shows that the qualitative nature of w is independent of the choice of w_i for all redshifts.

3.2 Minimum Energy

The detectability of a given FRB depends on the amount of total energy received by the telescope from the source. The minimum total energy E_{min} required to detect FRBs, is given by

$$E_{min} = (9.55 \times 10^{27}) \frac{4\pi r^2 F_l}{\bar{\phi}(z)B(\vec{\theta})} \sqrt{\frac{w}{1 \text{ ms}}} \quad (5)$$

where F_l is the limiting fluence, which further depends on the minimum signal to noise ratio S/N of the observation and the rms noise of the telescope for 1 ms observation. We consider $S/N = 10$ here. Here, fluence is defined as the time integral of flux density. As FRBs are one-off bursts of radiation, it is convenient to use fluence to quantify the integrated energy over the duration of the burst. The predicted pulse width w is scaled to 1 ms. The comoving distance r is estimated considering the standard Λ CDM cosmology (Spergel et al. 2003). $B(\vec{\theta})$ is the beam pattern, which is calculated using Eq. 1. $\bar{\phi}(z)$ is the emission line profile averaged over frequency, which is normalized by considering FRB 110220 as the reference event and the estimated total energy of the FRB as the reference energy $E_0 = 5.4 \times 10^{33}$ J. We have used F_l in Jy ms, r in Gpc, ν in MHz and E_{min} in J.

Figure 2 shows E_{min} as a function of z assuming the detected FRBs located at the beam center of OWFA, UTMOST and CHIME, expressed in units of E_0 . The different plots in a row correspond to different values of the spectral indices α , spanning a large range ($-3 \leq \alpha \leq 5$), where the flux $S(\nu) \propto \nu^{-\alpha}$ and a fixed $w_i = 1$ ms. E_{min} depends on the rms noise of observation and the predicted pulse width (w) of FRBs (Eq. 5). The values of w are the same for all phases of the OWFA with different beam formations but the rms noises are different. Therefore, the values of E_{min} are also different. Similar variations are also observed for UTMOST and CHIME. Incoherent and coherent single beam formation along with the two scattering models are shown in the top and bottom panels of the figure. For OWFA, UTMOST and CHIME, the predicted pulse widths increase very sharply for the scattering model I in comparison to the scattering model II, hence E_{min} also increases accordingly.

Figure 3 shows the results for OWFA Phase I and Phase II with coherent multiple beam formation and ORT Legacy System. The qualitative nature of Fig. 3 and Fig. 2 are similar. The dotted horizontal lines in both the figures are for $E_{min} = E_0$. Assuming that all FRBs have equal total energy $E \approx E_0$, the intersection of the curves with the dotted lines gives a useful

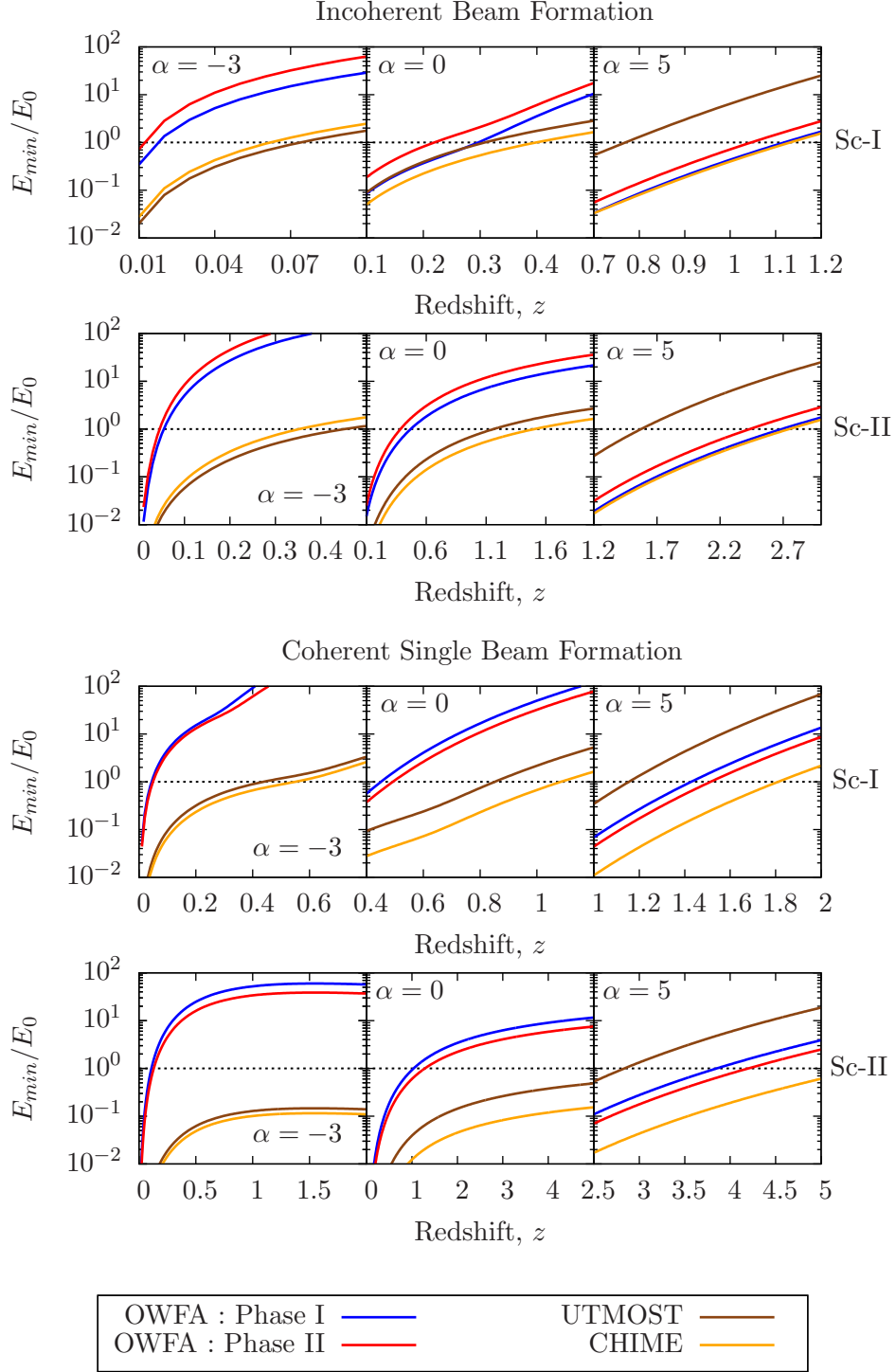


Figure 2: The minimum total energy E_{min} required to detect a FRB at a redshift z at the beam center of OWFA with its different phases and different values of the spectral indices α , i.e. $S(\nu) \propto \nu^{-\alpha}$, ($-3 \leq \alpha \leq 5$) in units of reference energy E_0 . The top and bottom panels correspond to incoherent beam formation and coherent Single beam formation modes. The first and second halves of each panel correspond to scattering model I (Sc-I) and scattering model II (Sc-II) respectively. We consider $w_i = 1$ ms.

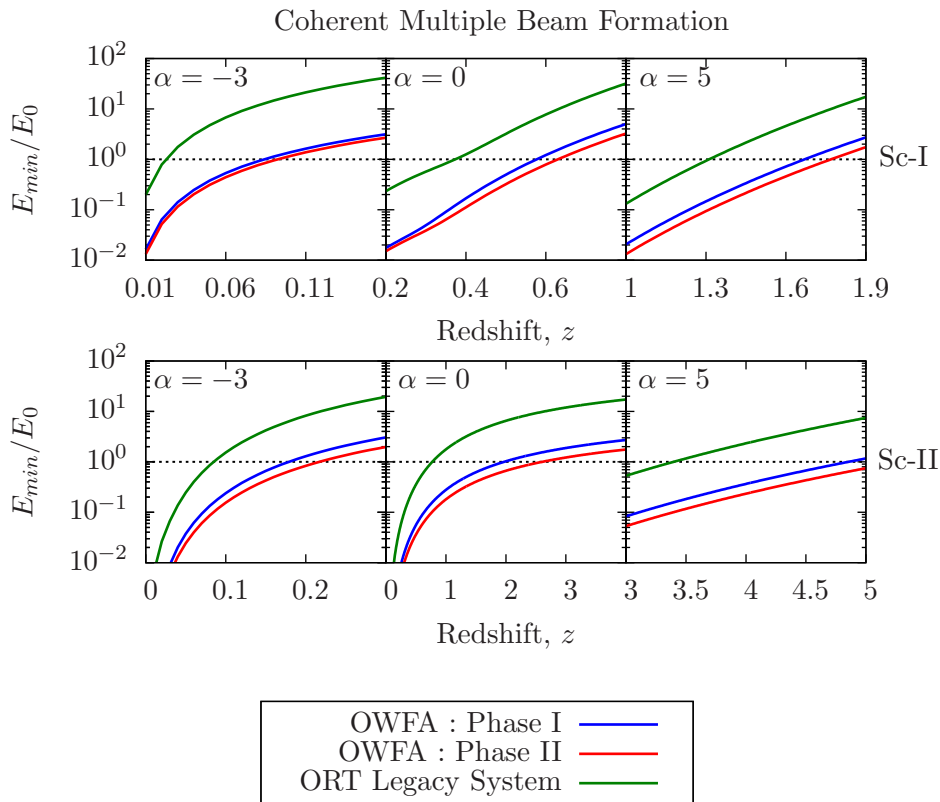


Figure 3: Similar to Fig. 2, but only for OWFA Phase I and Phase II with coherent multiple beam formation mode. The green line represents E_{min} for ORT Legacy System.

indication of the redshift up to which the telescope is sensitive enough to detect FRBs. This is denoted here as the cut off redshift z_c .

We first discuss the results for the incoherent beam formation mode, as shown in Fig. 2. For $\alpha = -3$, the cutoff redshifts are typically small for the scattering model I, while for scattering model II, the cutoff redshifts are quite feasible for both UTMOST and CHIME. For $\alpha = 5$, the curves corresponding to CHIME and OWFA Phase I overlap for both the scattering models. We find here that the values of z_c for UTMOST are small in comparison to others for both the scattering models. Coherent single beam formation, with $\alpha = 5$, also exhibits a similar feature.

Now we discuss the results for coherent single beam formation mode as shown in Fig. 2. For the scattering model I, the nature of the curves are quite similar to that of incoherent beam formation. For the scattering

model II with $\alpha \leq 0$, we do not have any cut off redshift for UTMOST and CHIME. It shows that both these telescopes can in principle probe FRBs out to arbitrarily high redshifts. Figure 3 shows that the cut off redshifts for the ORT Legacy System are always small compared to others. The other features of Fig. 3 are quite similar to Fig. 2. For the rest of the analysis we ignore the negative values of α , as it is consistent with currently available observational constraints. We repeated the entire analysis with $w_i = 0.5$ ms and 2 ms and find that at low redshift ($z \ll z_c$), there is a small deviation between the curves but overall there is no change in z_c (though not shown in Fig. 2 and Fig. 3). Therefore, henceforth, we shall use the value of intrinsic pulse width $w_i = 1$ ms.

3.3 Redshift Distribution

We now consider a quantity, N_{det} , which is total number of events expected to be detected for an observation time T . This quantity is obtained by integrating the comoving number density of FRBs $n(E, w_i, z)$ over energy, pulse width, the solid angle subtended by the telescope beam and redshift. The quantity N_{det} is given by

$$N_{det}(T) = T \int dz \frac{dr}{dz} \left(\frac{r^2}{1+z} \right) \int d\Omega \int dw_i \int_{E_{min}(z)}^{\infty} dE n(E, w_i, z) \quad (6)$$

where, $n(E, w_i, z)$ is the comoving number density of FRBs. The redshift integral is going up to the cut off redshift z_{cut} . N_{det} depends on the beam pattern of the telescope. We assume the sampling time of the telescope to be ≤ 1 ms so that the FRB signal is resolved. The cut off redshift z_c does not depend on the intrinsic pulse width w_i of the source and we assume here that all FRBs have the same intrinsic pulse width $w_i = 1$ ms. We further assume that $n(E, w_i, z)$ does not evolve with redshift, so n is solely a function of E . As the emission mechanism and the energy distribution of FRBs remain unknown, we consider two possible energy distribution functions, viz. a Delta function and a Schechter luminosity function. For the Delta function, we assume that all FRBs have the same energy that is equal to the reference energy $E_0 = 5.4 \times 10^{33}$ J, whereas in the Schechter luminosity function, an energy spread is allowed, is given by,

$$n(E, w_i, z) = \frac{n_0}{E_0} \left(\frac{E}{E_0} \right)^\gamma \exp \left(-\frac{E}{E_0} \right) \quad (7)$$

where the normalization constant n_0 is a free parameter, which is estimated by considering the detection of four FRBs during an effective observation time of 298 days with a single beam of the Parkes radio telescope (Thornton et al. 2013). We consider the exponent γ in the range $-2 \leq \gamma \leq 2$.

For a negative exponent ($\gamma < 0$), we fix the lower cut off of the energy as $E_0/100$ to normalize the function. The redshift distribution of FRBs refers to the variation of fraction of predicted events ($\Delta N_{det}/N_{det}$) with redshift z . Here ΔN_{det} is the number of events, which are expected to be detected over a redshift bin (z_{bin}) and N_{det} is the total number of events, expected to be detected over a redshift range ($0 \leq z \leq z_{max}$). We consider $z_{bin} = 0.1$ and $z_{max} = 5$.

Figure 4 shows $\Delta N_{det}/N_{det}$ as a function of z with $z_{bin} = 0.1$ and $0 \leq \alpha \leq 5$ for OWFA Phase II with different beam formation modes and energy distribution models of FRBs. The upper and lower halves correspond to the scattering models I and II, respectively, with $w_i = 1$ ms. The area under the curves gives an indicator of the total number of predicted FRBs for a particular beam formation mode of the OWFA with a particular energy distribution function of FRBs and a particular value of α . Figure 3 is very similar for all phases of OWFA, UTMOST and CHIME and are hence not shown here.

We find that the curves peak at a particular value of redshift z_p . The values of z_p increases with increasing α ($0 \leq \alpha \leq 5$). The stiffness and the peak values of the curves are dissimilar for different beam formation modes and for different scattering models. In the case of scattering model I, for the values of $\alpha = 0, 3$ and 5 , the approximate value of z_p are $0.3, 0.7$ and 1 respectively. The curves corresponding to the Delta function and the Schechter luminosity function with a positive exponent ($\gamma \geq 0$), are almost overlapping, whereas the curves for a negative exponent ($\gamma < 0$) are different. The area under the curves of the Schechter luminosity function with $\gamma = -2$ are small and the corresponding peak values are low. The highest peak value of the curves is maximum (~ 0.25) for the IA beam formation mode with $\alpha = 0$ and minimum (~ 0.08) for CA-MB beam formation mode with $\alpha = 5$. For the scattering model II, Fig. 3 shows that we can expect to detect FRBs at higher redshifts but we estimate a cut off $z = 5$. Here all the plots are similar, only the plots for IA beam formation mode with $\alpha = 0$ are slightly different. The curves are almost flat with low peak values for $\alpha > 0$. The curves corresponding to different energy distribution functions of FRBs are overlapping with each other. The highest peak value of the curves and the area under the curves for the Schechter luminosity function with $\gamma = -2$, are similar to those of the scattering model I.

3.4 Event rate

Finally, we consider FRB detection rates for a telescope with given parameters. We use Eq. 6 to estimate this quantity for the OWFA, UTMOST and CHIME; in each case for different beam formations. We use the detection rates from Thornton et al. (2013) as our reference.

Figures 5 and 6 show the FRB detection rates (day^{-1}) as a function of

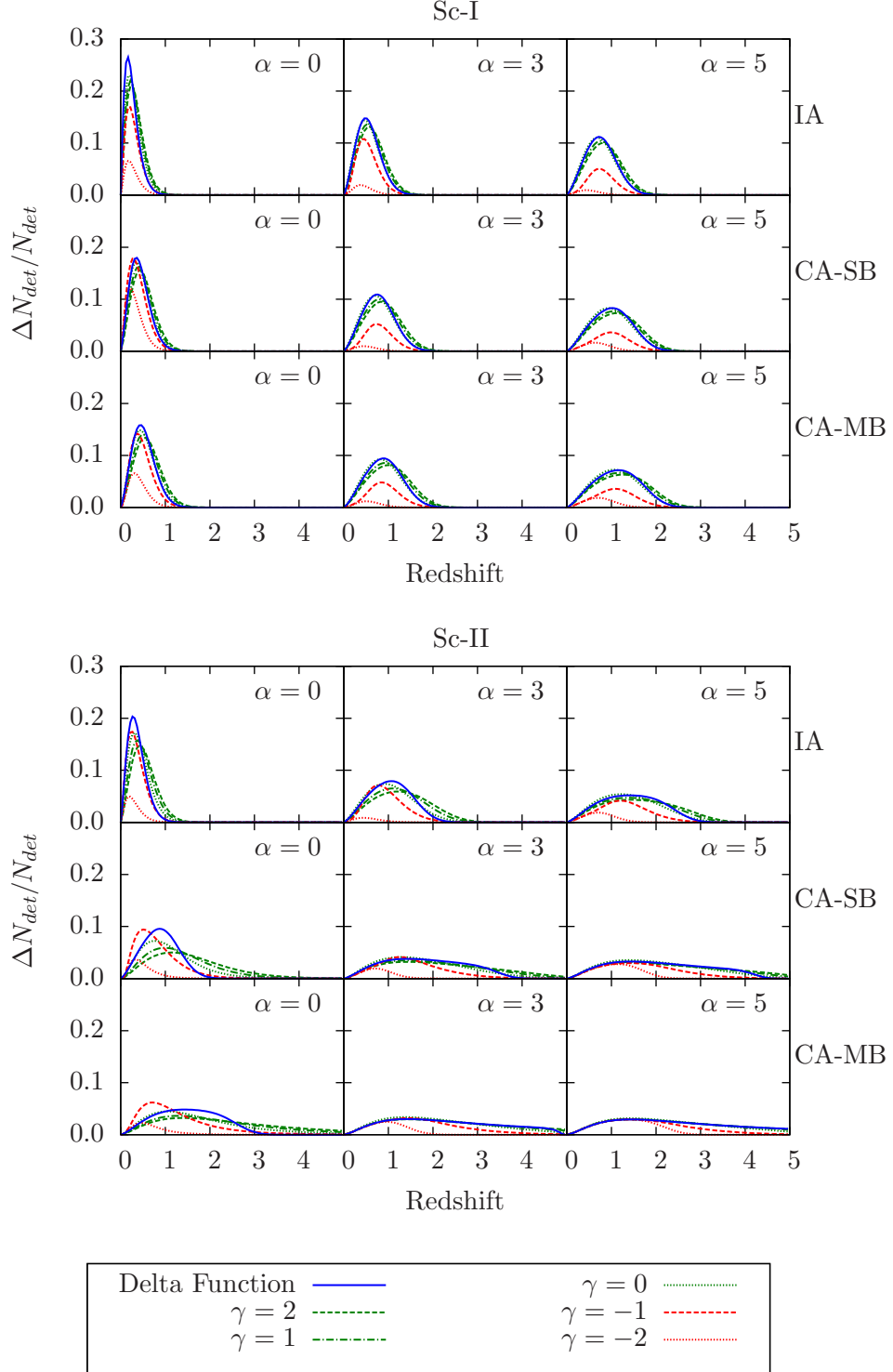


Figure 4: The fraction of predicted FRBs over the bin on redshift axis ($z_{bin} = 0.1$) for OWFA Phase II with different beam formation modes and different energy distribution functions of FRBs. Different panels in a row correspond to different values of α ($0 \leq \alpha \leq 5$). Upper and lower halves correspond to scattering model I (Sc-I) and scattering model II (Sc-II) respectively with $w_i = 1$ ms.

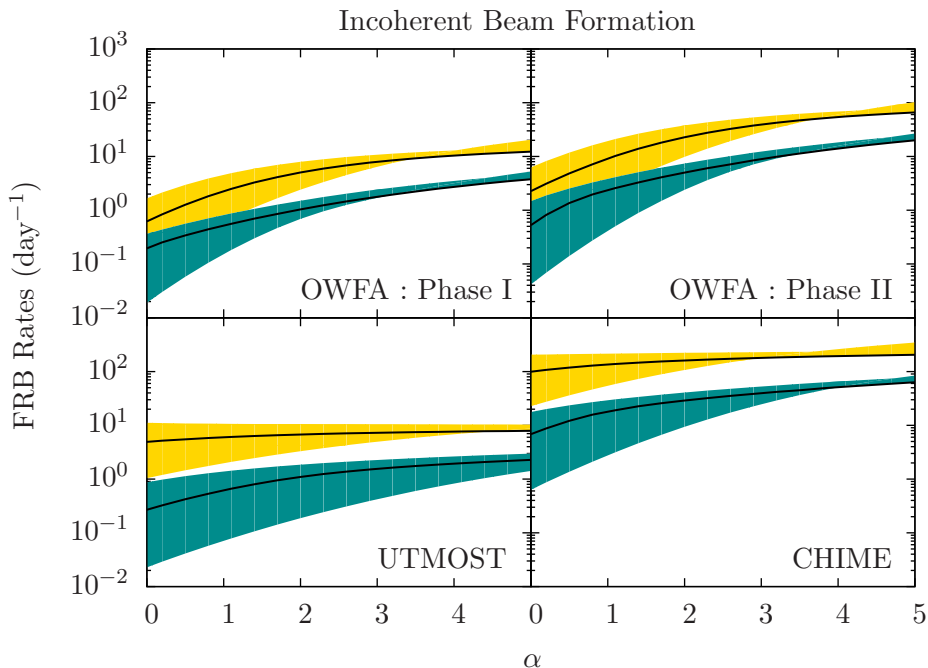


Figure 5: The number of FRBs expected to be detected per day by using OWFA, UTMOST and CHIME with incoherent beam formation. The yellow and green regions correspond to scattering model I (Sc-I) and scattering model II (Sc-II) respectively. Solid black lines denote Delta function, while the boundaries of the regions enclose the curves corresponding to the Schechter luminosity function with exponent in the range $-2 \leq \gamma \leq 2$.

α for OWFA, UTMOST and CHIME with incoherent and coherent Single beam formations, whereas in Fig. 7 we show these rates for OWFA Phase I and Phase II, for coherent multiple beam formation and the ORT Legacy System. The yellow and green solid regions represent the scattering models I and II, respectively. The solid black lines refer to the Delta function whereas the boundaries of the regions enclose the curves representing the Schechter luminosity function with exponents in the range $-2 \leq \gamma \leq 2$. The detection rates (day^{-1}) increase, with increasing α ($\alpha > 0$). The detection rates corresponding to the scattering model I are large in comparison to the that of scattering model II. The approximate numbers of FRBs expected to be detected per day for OWFA, UTMOST and CHIME with the consideration of Delta function as the energy distribution function of FRBs and $\alpha = 1.4$ are tabulated in Table 2 for comparison.

It is easily shown that a large number of FRBs are likely to be detected by OWFA with coherent multiple beam formation rather than coherent single beam formation. In particular we expect to detect ~ 100 FRBs per day

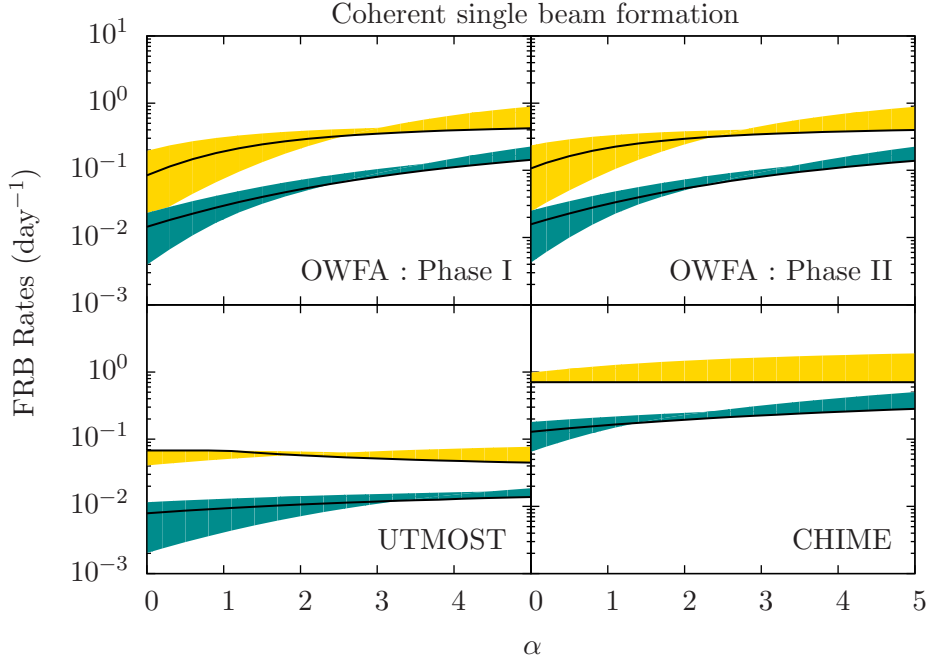


Figure 6: Same as Fig. 5 with coherent single beam formation.

Telescope	Beam Formation	Number of FRBs per day	
		Scattering Model I	Scattering Model II
ORT Legacy System	–	0.14	0.03
OWFA Phase I	IA	3.25	0.70
	CA-SB	0.23	0.04
	CA-MB	14.85	2.31
OWFA Phase II	IA	13.74	3.34
	CA-SB	0.25	0.04
	CA-MB	103.12	15.94
UTMOST	IA	6.38	0.81
	CA-SB	0.06	0.01
CHIME	IA	144.65	22.42
	CA-SB	0.71	0.17

Table 2: The approximate number of FRBs expected to be detected per day is estimated by considering Delta function as the energy distribution function of FRBs with $\alpha = 1.4$.

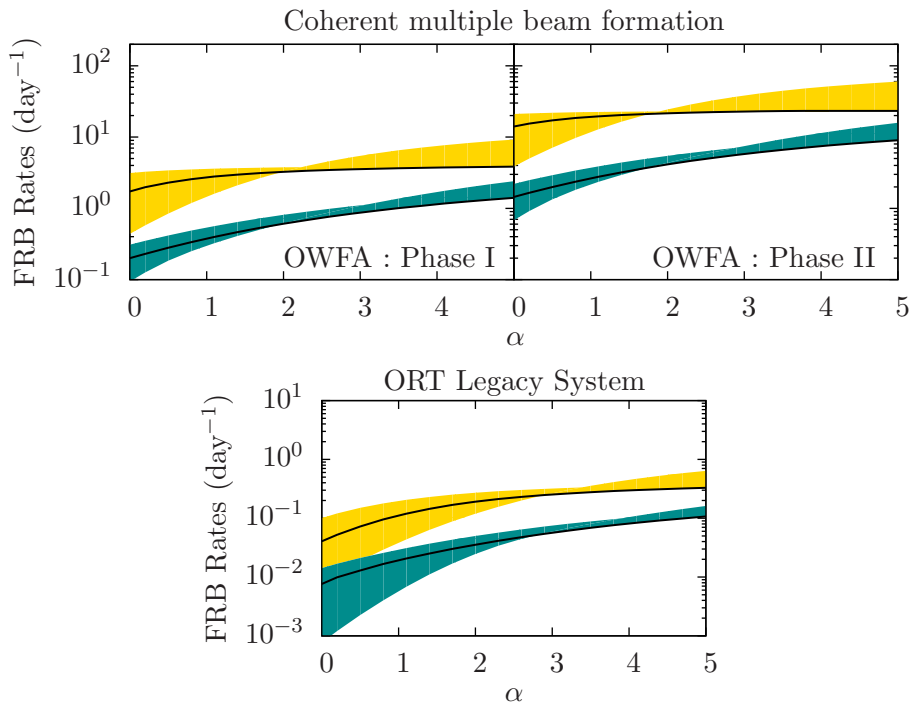


Figure 7: Same as Fig. 5. The upper panels denote OWFA Phase I and Phase II with coherent multiple beam formation. The lower panel denotes ORT Legacy System.

with OWFA Phase II in the case of coherent multiple beam formation. The detection per day for OWFA Phase II are large compared to the that for UTMOST. Table 2 shows that the detection per day is even larger for CHIME with incoherent beam formation. This is not surprising since CHIME has a large field of view compared to others. However, as we emphasized earlier, these three telescopes operate in different frequency ranges and hence complementary. The approximate numbers for FRBs detections are summarized in Table 2 for the specific case of $\alpha = 1.4$ to allow further meaningful comparison.

4. Summary & Conclusions

We have presented a detailed analysis of FRB detection rates for different phases of OWFA using a generic formalism prescribed in our previous work (Bera et al. 2016). We compare the results with two other cylindrical radio telescopes, UTMOST and CHIME. The formalism of the event rate prediction is followed by the predicted pulse widths of FRBs, the minimum total energy required to detect events and the redshift distribution of FRBs. We

consider three different kinds of beam formations for OWFA; viz. incoherent, coherent single and coherent multiple beam formations.

The predicted pulse widths of FRBs are estimated by considering two different scattering models and an arbitrary intrinsic pulse width. The contributions from residual dispersion smearing and cosmic expansion are also taken into account. We find that the intrinsic pulse width of FRB (w_i) makes insignificant contribution to the predicted pulse width for all redshifts, whereas scatter broadening however tend to dominate the pulse width. The pulse width vs z variation is steeper for the scattering model I than that of scattering model II. The predicted pulse width for UTMOST and CHIME are smaller than that for OWFA, however the qualitative nature of the curves are similar.

The detection prospects of FRBs depend on the amount of the total energy received by the telescope from the source. We find the OWFA will be capable of detecting FRBs with $\alpha \gtrsim 0$. However, there is no cut off in redshift for UTMOST and CHIME, which is due to their higher operating frequencies.

We estimated the redshift distribution of the predicted FRBs for OWFA, UTMOST and CHIME. The qualitative nature of the curves are similar for all the three telescopes. We however find that the curves peak at a certain redshift (z_p) in the range $0.3 \leq z_p \leq 1$ for scattering model I, whereas the curves are almost flat extending up to a high redshift for scattering model II. As a result the expected events per redshift range is low.

Finally, we have estimated the detection rates of FRBs for different phases of OWFA, considering different kinds of beam formation scenarios and compared them with the rates estimated for UTMOST and CHIME. The detection rates primarily depend on two important factors, the sensitivity and the field of view. The detection rate is higher for a telescope with a large field of view and a high sensitivity, and is qualitatively proportional to the product of these two factors. We find that the value of this product is maximum for OWFA Phase II in the coherent multiple beam formation mode. Our analysis predict that for OWFA Phase II, we can expect ~ 100 FRBs per day. The detection rates with the scattering model I are large compared to the that of scattering model II.

There are however some limitations of our analysis. The scattering mechanism in the intervening medium is still unknown. Cordes et al. (2016) showed that the scatter broadening is not proportional to DM for currently known sample of FRBs. Moreover, there is no unique and direct way to estimate the spectral index of FRBs. We have addressed this to a certain extent by considering both negative and as well as positive spectral indices. The energy distribution of FRBs is another important unknown and we have considered two possible energy distribution functions. Detection of FRBs in large numbers will therefore help us to constrain many of these uncer-

tainties and refine the of FRBs models including their energy and redshift distributions.

References

- Ali S. S. & Bharadwaj S. 2014, *Journal of Astrophysics and Astronomy*, 35, 157182
- Bera A., Bhattacharyya S., et al. 2016, *Monthly Notices of the Royal Astronomical Society*, 457, 2530
- Bhat N. D. R., Cordes J. M., et al. 2004, *The Astrophysical Journal*, 605, 759
- Bhat N. D. R., Chengalur J. N., et al. 2013, *The Astrophysical Journal Supplement Series*, 206, 1
- Caleb M., Flynn C., et al. 2016, *Monthly Notices of the Royal Astronomical Society*, 458, 718
- Cordes J. M., Wharton R. S., et al. 2016, *ArXiv e-prints*, 1605.05890
- Cordes J. M. & Lazio, T. J. W. 2002, *ArXiv e-prints*, 0207156
- Kulkarni S. R., Ofek E. O., & Neill J. D. 2015, *ArXiv e-prints*, 1511.09137
- Lorimer D. R., Bailes M., et al. 2007, *Science*, 318, 777
- Macquart J.-P. & Koay J. Y. 2013, *The Astrophysical Journal*, 776, 125
- Masui K., Lin H., et al. 2015, *Nature*, 528, 523
- Newburgh L. B., Addison G. E., et al. 2014, *SPIE Proceedings*, 9145
- Petroff E., Barr E. D., et al. 2016, *ArXiv e-prints*, 1601.03547
- Spergel D. N., Verde L., et al., 2003, *ApJS*, 148, 175
- Spitler L. G., Cordes J. M., et al. 2014, *The Astrophysical Journal*, 790, 101
- Spitler L. G., Scholz P., et al. 2016, *Nature Letter*, 531, 202
- Swarup G., Sarma N. V. G., et al. 1971, *Nature Physical Sciences*, 230, 185
- Subrahmanyan C. R., Chengalur J. N., et al. 2016, *In this Volume*
- Thornton D., Stappers B., et al. 2013, *Science*, 341, 53